Tunable exciton relaxation in vertically coupled semiconductor InAs quantum dots

Kushal C. Wijesundara, Juan E. Rolon, Sergio E. Ulloa, Allan S. Bracker, Daniel Gammon, and Eric A. Stinaff

Phys. Rev. B **84**, 081404 — Published 25 August 2011

DOI: 10.1103/PhysRevB.84.081404

Tunable exciton relaxation in vertically coupled semiconductor quantum dots

Kushal C. Wijesundara[1], Juan E. Rolon[1], Sergio E. Ulloa[1], Allan S. Bracker[2], Daniel Gammon[2], and Eric A. Stinaff[1,*]

[1] *Department of Physics and Astronomy, Nanoscale and Quantum Phenomena Institute, Ohio University, Athens, Ohio 45701-2979, USA*

[2] *Naval Research Laboratory, Washington, D.C. 20375, USA*

Tunable exciton relaxation rates are observed in individual vertically coupled semiconductor quantum dots (CQDs). An applied electric field is used to tune the energy difference between the spatially direct (SD) and indirect (SI) exciton in InAs CQDs. The intensity and lifetime of the SI exciton is found to vary as a result of wavefunction distribution, carrier tunneling and phonon mediated relaxation effects. This includes a modulation of the phonon relaxation rate between the SI and SD exciton, a consequence of momentum space restrictions resulting from the structure factor of the CQD.

PACS numbers: 78.67.Hc, 71.35.-y, 63.22.- m, 78.47.D-

*Corresponding author: stinaff@ohio.edu

Vertically coupled InAs quantum dots (CQDs) have received attention as a candidate for physical implementations of quantum information processing. This is due to their many attractive properties, including integration with existing semiconductor technology [1,2], the ability to use ultra-fast optoelectronic techniques for state manipulation [3-5], and the ease with which relevant properties can be engineered [6]. Increasingly sophisticated experiments have demonstrated the potential of excitons in these systems to satisfy the requirements of quantum computation [7,8]. However, in addition to relatively short radiative lifetimes, strong coupling to the environment often results in loss of coherence through acoustic phonon induced carrier relaxation. Therefore, the understanding and possible control of such mechanisms is of fundamental importance. Here we report the direct observation of tunable exciton relaxation dynamics in CQDs.

Dominant sources of exciton relaxation in a CQD include radiative recombination and relaxation into other states through a combination of phonon scattering and charge carrier tunneling. In contrast with higher dimensional structures [9], the discrete nature of the energy levels in low dimensional systems, such as quantum dots (QDs), significantly restricts the processes through which relaxation can occur [10]. In CQDs with exciton energy separation of only a few meV, the dominant phonon scattering mechanism that limits the lifetimes involves acoustic phonons [11-14]. However, there is the additional possibility of molecular states where the carrier wavefunction is spatially delocalized between the dots comprising the CQD system. This both reduces the electron-hole overlap and modifies the carrier-phonon interaction [15]. Theoretical investigations on the coupling between acoustic phonons, excitons and single particle bonding-antibonding states, have suggested that the acoustic phonon scattering rates can be enhanced or suppressed as a function of interdot separation and applied field, both in single and coupled QDs [16,17]. We observe clear evidence of such a modulation of the acoustic phonon mediated relaxation and find that the measured lifetime of the tunable indirect exciton (X_I) can be understood from the molecular character of the exciton states and the structure factor characteristics of the phonon scattering mechanism.

The samples consist of two coupled layers of epitaxially grown InAs QDs in a GaAs matrix [18-20]. The CQDs have been grown within the insulating region of an n-

type Schottky diode structure to allow for the application of an electric field where the top aluminum contact has apertures to optically isolate individual CQDs [21]. We are operating in a field range where the formation of negative trions is negligible and, since the diodes are operating in reverse bias, the only source of additional holes for the formation of a positively charged exciton state (X^+) is through the tunneling of electrons from the photogenerated excitons to the doped substrate [22,23]. The sample is kept at ~10 K, and excited with a mode locked Ti:Sapphire laser, with a pulse width of ~1.5 ps operating at 80 MHz. A 0.75 m spectrometer is used to disperse the signal while a silicon avalanche photodiode with temporal resolution of 500 ps along with standard time-resolve single photon counting electronics are used to acquire lifetimes.

One of the challenges in the measurement of X_I is the significantly reduced emission, relative to the direct exciton (X_D), due to the spatial separation of the electron and hole. Therefore we focused our study on CQDs with small barriers displaying signatures of hole level molecular wavefunction formation. Figure 1 shows a schematic representation of the relevant states and processes for the device structure and field range used in this study [6]. By reducing the applied electric field we can tune the $X_I - X_D$ energy separation from 0.8 to 19 meV by increasing the energy of the hole level in the top dot relative to the hole in the bottom dot. The hole in the bottom dot can be thought of as the lowest energy ground state (X_D) and the hole in the top dot as an excited state (X_I). Tuning of the relative hole energies with electric field also results in a shift from a more molecular-like to a more atomic-like state with increasing energy separation.

We observe a strong non-monotonic modulation of both the measured lifetime and intensity of X_I as its energy separation from X_D is increased, as seen in Fig. 2(a,b). At the anticrossing point both X_I and X_D are strictly molecular and the intensities and lifetimes are comparable, but as the energy separation increases the intensity of X_I first decreases to a minimum at a separation of ~6-8 meV, steadily increases to a local maximum at ~12 meV, and then again decreases. The lifetimes are found to have a similar modulated behavior, increasing first to a maximum at ~3-4 meV, decreasing to a minimum at ~6-8 meV, coincident with the intensity minimum, increasing to another maximum at ~14 meV before again decreasing. This behavior was observed in three different CQDs where the indirect line could be clearly measured. In each of these CQDs

the first intensity minimum and lifetime maximum/minimum beyond the anticrossing occurred at similar direct-indirect energy separations. However, the position of the subsequent maxima varied between CQDs, as seen in Fig. 2(d,e), but was found to always coincide with the onset of the positively charged exciton molecular anticrossing signature [21].

The observed non-monotonic trend of the intensity and lifetime strongly suggest that the X_I relaxation mechanism has contributions not only of radiative recombination but also of nonradiative relaxation. The pure radiative oscillator strength of X_I is a monotonic function of the decreasing electron-hole overlap with applied field, and any modulation of the measured lifetime should arise from nonradiative relaxation channels that satisfy two conditions: (i) possess transition matrix elements that are sensitive to the hole delocalization as a function of applied field, (ii) are energetically allowed within the moderate energy separation between the initial X_I state and final X_D state. This strongly suggests a relaxation assisted by acoustic phonon emission via scattering mostly with the hole component of the exciton.

In order to separate the different contributions to the measured relaxation rates (i.e. X_I lifetimes) we performed lifetime measurements of X_D with resonant excitation into X_I, eliminating the contribution from carrier tunneling into charged exciton states. Therefore, if the laser is resonantly tuned to the X_I energy, the formation of a different charge state is forbidden due to the Coulomb correction of the additional charge. The rate equations for this simpler process are given by

$$\frac{dN_I}{dt} = -R_I N_I - \gamma_p N_I + G, \qquad \frac{dN_D}{dt} = -R_D N_D + \gamma_p N_I, \tag{1}$$

where R_D and R_I are, respectively, the rates in which X_D and X_I are lost to radiative recombination and tunneling to the contacts, γ_p is the nonradiative phonon relaxation from X_I to X_D, and G is the generation rate of X_I. Although we can not extract the purely radiative recombination rate this does not affect the ability to determine the phonon contribution. The resulting time dependence for the direct N_D, and indirect N_I, exciton normalized populations is given by

$$N_I = e^{-\Gamma_I t}, \qquad N_D = (1+\alpha)e^{-\Gamma_D t} - \alpha e^{-\Gamma_I t}, \tag{2}$$

where, $\Gamma_D = R_D$, $\Gamma_I = R_I + \gamma_p$, and $\alpha = \gamma_p / (R_I - R_D + \gamma_p)$.

From fits to the bi-exponential behavior in the X_D lifetime it is seen that the X_I lifetimes, $\tau_I = (\Gamma_I)^{-1}$, are identical under resonant and non-resonant excitation only up to where the X^+ states become noticable in PL spectra [Fig. 3(a)]. At this point, for energy separations larger than 14 meV, the resonant lifetimes diverge from the non-resonant, increasing to nearly 4 ns. This demonstrates the effect of the X^+ formation on the non-resonant lifetimes at large energy separations. The inclusion of a X^+ formation rate, γ_t, simply results in an additional term in the total X_I rate, $\Gamma_I' = R_I + \gamma_p + \gamma_t$. This, along with Eq. (2), allows us to directly extract, from the data, each contribution to the overall lifetime of X_I as plotted in Fig. 4.

To understand the physics of the extracted relaxation rates, we have constructed a model for X_I relaxation, including radiative recombination and acoustic phonon scattering for an asymmetric CQD [24]. The exciton states are constructed from product states of the lowest energy single particle states confined in 3D parabolic potentials matched to band edges of the QD and host materials. The radiative recombination is given in the dipole approximation by

$$R_I = \frac{\sqrt{\varepsilon_R} E_{exc}^3 O_{eh}^2 P_{cv}^2}{3\pi c^3 \hbar \varepsilon_0}, \tag{3}$$

where P_{cv} is the interband dipole moment in the QD material, while E_{exc} is the X_I energy and O_{eh} the electron-hole overlap, both of which depend on the applied electric field. We have found that to match the experimentally observed radiative recombination rates it is necessary to assume a delocalization of the electron across the CQD of 9-11% on the top dot. This is reasonable for small barriers such as in these CQDs. The acoustic phonon relaxation rate can be obtained from the expression

$$\gamma_p = \frac{2\pi}{\hbar} \sum_{v\mathbf{q}} |M_V(\mathbf{q})|^2 \left| \langle X_D | e^{i\mathbf{q}.\mathbf{r}} | X_I \rangle \right|^2 \delta(\Delta E - \hbar c_{vq} q), \tag{4}$$

where the sum runs over all acoustic phonon polarizations, and it includes contributions from deformation potential and piezoelectric scattering (as defined by the scattering matrix element M_v). Phonon emission takes place whenever a phonon mode energy $\hbar c_{vq} q$ matches the field-dependent energy separation, $\Delta E = \sqrt{(eFd)^2 + 4t_h^2}$, where c_{vq} is the corresponding sound velocity for mode v, d is the interdot distance in the CQD, and t_h

is the hole tunneling amplitude. The scattering matrix element is field independent but exhibits a q-dependence that varies with the phonon coupling mechanism [17]. On the other hand, the structure factor $\left|\langle X_D | e^{i\mathbf{q}.\mathbf{r}} | X_I \rangle\right|^2$ does exhibit a strong electric field dependence, as the exciton states evolve from the molecular to the spatially separated state of the hole. The structure factor can be seen as the Fourier transform of the field-dependent charge density distribution of the exciton molecular states involved in the relaxation. Given the axial symmetry and strong dot confinement potentials, the phonon emission is dominated by the interdot separation. To highlight this dependence, we calculated the structure factor as a function of ΔE (i.e. applied electric field) and as a function of the axial component of the phonon wave vector q_z. In performing this calculation we have separated the phonon wave vector into in-plane and axial components, which together with energy conservation results in

$$q_z = \frac{\Delta E}{\hbar c_{qv}} \cos\theta \,, \quad q_{||} = \frac{\Delta E}{\hbar c_{qv}} \sin\theta \,, \tag{5}$$

where θ is the polar angle respect to the growth direction. Phonon emission closer to the in-plane direction ($\theta \sim \pi/2$) gives a weak contribution, and the deformation potential contributions are generally larger than the piezoelectric contributions for this system, especially at higher energy separation. The structure factor is maximum for $\theta \sim 0$ (or π) and exhibits modulations with peaks occurring whenever q_z is an odd multiple of π/d, indicating a clear phase relationship between the phonon axial wave vector and the hole wave function along the growth direction.

The phase relationship between q_z and the hole wave function can be either controlled with the interdot separation d or with the applied field, as it tunes the energy separation ΔE. The coincidence of the line $q_z d(\Delta E)$ in Fig. 4(inset) with maxima in the structure factor reveal which values of ΔE result in efficient relaxation, manifested as periodic peaks in the phonon relaxation rate (γ_p) as a function of ΔE. Thermal population effects ($kT \sim$ 1-2 meV) giving rise to phonon absorption as well as emission which may account for part of the suppression of the first peak ($\Delta E \sim$ 2.6 meV). For $\Delta E \sim$ 6.2 meV, when $q_z d$ has a value of 3π, we observe a clear peak in γ_p that agrees well with theory

[Fig. 4]. The magnitude and decreasing trend in the phonon rates are also consistent with theoretical predictions. This is an indication that the non-monotonic features of the phonon mediated carrier relaxation into the lowest energy, X_D state results from a modulation in the allowed momentum due to the real-space structure factor of the CQD. Despite the suppression of the first peak, the appearance of a non-monotonic modulation of the lifetimes cannot be accounted for by the purely monotonic contributions of charge tunneling and wavefunction overlap. Therefore, by engineering the real-space composition of coupled nanostructures it may be possible to dramatically extend (or shorten) the lifetimes of excitonic states.

We have observed non-monotonic phonon relaxation rates whose features are strongly dependent on the hole wave function confinement along the lateral and vertical directions, which in turn are determined by the entire CQD structural parameters such as the interdot distance, dot heights and lateral size. Our results confirm that the lifetimes of indirect excitons in CQDs can be controlled with an external electric field. Our results also suggest that since the structure factor is the Fourier transform of the excitonic charge density distribution, the measured modulated phonon relaxation rates can provide additional insight into the geometry and composition of QD structures. The ability to tune the relaxation rates of excitons could prove extremely useful to applications ranging from quantum information to optoelectronics.

This work was supported by the NSF (DMR-1005525, MWN/CIAM and PIRE grants), NSA/LPS, MURI/Army, and the Ohio University CMSS and NQPI programs. We thank Alexander Govorov for helpful discussions.

[1] T. D. Germann, A. Strittmatter, J. Pohl, U. W. Pohl, D. Bimberg, J. Rautiainen, M. Guina, and O. G. Okhotnikov, Appl. Phys. Lett. **93**, 051104 (2008).

[2] Ilya Fushman, Edo Waks, Dirk Englund, Nick Stoltz, Pierre Petroff, and Jelena Vučković, Appl. Phys. Lett. **90**, 091118 (2007).

[3] M. V. Gurudev Dutt, Jun Cheng, Yanwen Wu, Xiaodong Xu, D. G. Steel1, A. S. Bracker, D. Gammon, Sophia E. Economou, Ren-Bao Liu, and L. J. Sham, Phys. Rev. B **74**, 125306 (2006).

[4] J. Berezovsky, M. H. Mikkelsen, N. G. Stoltz, L. A. Coldren, and D. D. Awschalom, Science **320**, 349 (2008).

[5] Danny Kim, Samuel G. Carter, Alex Greilich, Allan S. Bracker & Daniel Gammon, Nature Physics **7**, 223 (2011).

[6] A. S. Bracker, M. Scheibner, M. F. Doty, E. A. Stinaff, I. V. Ponomarev, J. C. Kim, L. J. Whitman, T. L. Reinecke, and D. Gammon, Appl. Phys. Lett. **89**, 233110 (2006).

[7] Xiaoqin Li, Yanwen Wu, Duncan Steel, D. Gammon, T. H. Stievater, D. S. Katzer, D. Park, C. Piermarocchi, and L. J. Sham, Science **301**, 809 (2003).

[8] Y. Benny, S. Khatsevich, Y. Kodriano, E. Poem, R. Presman, D. Galushko, P. M. Petroff, and D. Gershoni, Phys. Rev. Lett. **106**, 040504 (2011).

[9] B. Krummheuer, V. M. Axt, and T. Kuhn, Phys. Rev. B **65**, 195313 (2002).

[10] T. Takagahara, Phys. Rev. B **60**, 2638 (1999).

[11] N. H. Bonadeo, Gang Chen, D. Gammon, D. S. Katzer, D. Park, and D. G. Steel, Phys. Rev. Lett. **81**, 2759 (1998).

[12] W. Langbein, P. Borri, and U. Woggon, V. Stavarache, D. Reuter, and A. D. Wieck, Phys. Rev. B **70** 033301 (2004).

[13] P. Borri, W. Langbein, U. Woggon, M. Schwab, and M. Bayer, S. Fafard, Z. Wasilewski, and P. Hawrylak, Phys. Rev. Lett. **91**, 267401 (2003).

[14] G. Ortner, R. Oulton, H. Kurtze, M. Schwab, D. R. Yakovlev, and M. Bayer, S. Fafard, Z. Wasilewski, and P. Hawrylak, Phys. Rev. B **72**, 165353 (2005).

[15] T. Nakaoka, E. C. Clark, H. J. Krenner, M. Sabathil, M. Bichler, Y. Arakawa, G. Abstreiter, and J. J. Finley, Phys. Rev. B **74**, 121305(R) (2006).

[16] U. Bockelmann, Phys. Rev. B **50**, 17271 (1994).

[17] Andrea Bertoni, Massimo Rontani, Guido Goldoni, Filippo Troiani, and Elisa Molinari, Appl. Phys. Lett. **85**, 4729 (2004).

[18] I. N. Stranski and V. L. Krastanow, Akad. Wiss. Lit. Mainz Math.-Natur. Kl. IIb **146**, 797 (1939).

[19] G. S. Solomon, J. A. Trezza, A. F. Marshall, and J. S. Harris, Jr., Phys. Rev. Lett. **76**, 952 (1996).

[20] Z. R. Wasilewski, S. Fafard, and J. P. McCaffrey, J. Cryst. Growth **201**, 1131 (1999).

[21] E. A. Stinaff, M. Scheibner, A. S. Bracker, I. V. Ponomarev, V. L. Korenev, M. E. Ware, M. F. Doty, T. L. Reinecke, and D. Gammon, Science **311**, 636 (2006).

[22] Dirk Haft, Richard J. Warburton, Khaled Karrai, Serge Huant, Gilberto Medeiros-Ribeiro, Jorge M. Garcia, Winston Schoenfeld, and Pierre M. Petroff, Appl. Phys. Lett. **78**, 2946 (2001).

[23] M. Ediger, P. A. Dalgarno, J. M. Smith, B. D. Gerardot, R. J. Warburton, K. Karrai, and P. M. Petroff, Appl. Phys. Lett. **86**, 211909 (2005).

[24] Simulation parameters: Interdot distance, d = 7 nm; hole Gaussian wavefunctions FWHMs (in-plane, vertical) directions, (3.5,2.6) nm Bottom QD, and (8.2,2.3) nm Top QD respectively; hole deformation potential, D_h = 950 meV; phonon speeds, c_{LA}, c_{TA} = 7, 3.2x10^3 m/s; crystal density, ρ = 5600 kg/cm^3, piezoelectric constant, h_{PZ} = 12.65 V/m; tunneling matrix elements, t_h, t_e = 0.43,20 meV; Top QD electron level detuning Δ_e = 60 meV, resulting in 9-11% electron delocalization on Top QD.

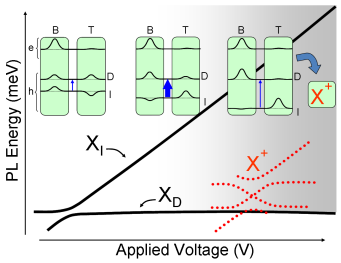

FIG. 1 (color online). Schematic representation of the states and processes. The green rectangles represent the bottom (B) and top (T) quantum dots. We assume the electron is mostly isolated in the bottom dot and that the holes form molecular states, labeled D and I, resulting in spatially direct (X_D) and indirect (X_I) excitons. The phonon mediated relaxation from the X_I to X_D states (blue solid arrows), varies with field. Eventually the formation of positively charged excitons (X^+) begins to dominate, represented by the grey shading.

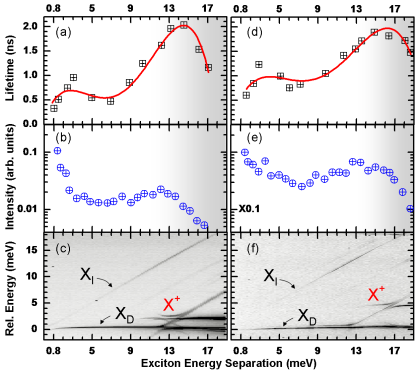

FIG. 2 (color online). (a) X_I lifetime relative to the exciton energy separation. The grey shading (a, b, d, and e) indicates the increasing X^+ photoluminescence (PL) intensity, similar to Fig. 1. The red line (polynomial fit) is a guide to the eye. (b) X_I intensity, normalized to compensate for the overall increase in PL intensity at larger energy separations. (c) PL spectra, as a function of electric field, relative to the neutral exciton anticrossing and energy separation between X_I and X_D. (d-f) Same as (a-c) for a second CQD with different X^+ energies.

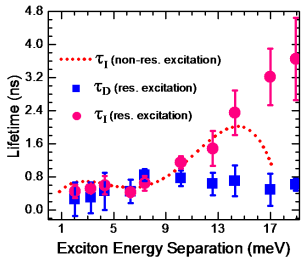

FIG. 3 (color online). Lifetime measurements resulting from resonant excitation at the X_I energy. The lifetimes, τ_D (blue squares), and τ_I (red circles) extracted from bi-exponential fits to the measured X_D lifetime. Lifetimes for τ_I agree with the non-resonant lifetimes in Fig. 2 (dotted polynomial fit) for exciton energy separations <14 meV. At higher energy separation the resonant τ_I deviates from the non-resonant lifetimes due to the absence of the X^+ formation.

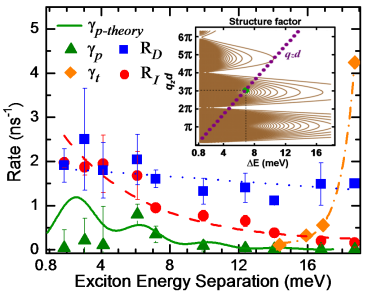

FIG. 4 (color online). Rates extracted from the data for R_D, R_I and the non-radiative contributions to the exciton lifetimes (phonon (γ_p) and trion formation (γ_t)). The green (solid) line is the theoretical total phonon-mediated relaxation rate, sum of the deformation potential and piezoelectric channels, of the X_I state ($\gamma_{p\text{-}theory}$). The blue (dotted) line is a linear fit to R_D, the red (dashed) line is an exponential fit to the experimental R_I, the orange (dash-dot) line is an exponential fit to γ_t. Inset shows the structure factor contour plot as function of exciton energy separation and axial component of the phonon wave vector for fixed interdot distance d, and axial emission at $\theta=0$.